

Disrupted core-periphery structure of multimodal brain networks in Alzheimer's Disease

Jeremy Guillon^{1,2}, Mario Chavez³, Federico Battiston^{10,3,2}, Yohan Attal⁴, Valentina La Corte^{5,6,7}, Michel Thiebaut de Schotten¹, Bruno Dubois⁸, Denis Schwartz⁹, Olivier Colliot^{2,1}, and Fabrizio De Vico Fallani^{2,1,*}

¹Institut du Cerveau et de la Moelle Epiniere, ICM, Inserm, U 1127, CNRS, UMR 7225, Sorbonne Universite, F-75013, Paris, France

²Inria Paris, Aramis project-team, F-75013, Paris, France

³CNRS, UMR 7225, F-75013, Paris, France

⁴MyBrain Technologies, Paris, France

⁵Department of Neurology, Institut de la Memoire et de la Maladie d'Alzheimer - IM2A, Paris, France

⁶INSERM UMR 894, Center of Psychiatry and Neurosciences, Memory and Cognition Laboratory, Paris, France

⁷Institute of Psychology, University Paris Descartes, Sorbonne Paris Cite, France

⁸Institut de la Mémoire et de la Maladie d'Alzheimer - IM2A, AP-HP, Sorbonne Université, Paris, France

⁹Institut du Cerveau et de la Moelle Epiniere, ICM, Inserm U 1127, CNRS UMR 7225, Sorbonne Universite, Ecole Normale Superieure, ENS, Centre MEG-EEG, F-75013, Paris, France

¹⁰Department of Network and Data Science, Central European University, Budapest 1051, Hungary

*Corresponding author

December 10, 2018

Abstract

In Alzheimer's disease (AD), the progressive atrophy leads to aberrant network reconfigurations both at structural and functional levels. In such network reorganization, the core and peripheral nodes appear to be crucial for the prediction of clinical outcome due to their ability to influence large-scale functional integration. However, the role of the different types of brain connectivity in such prediction still remains unclear. Using a multiplex network approach we integrated information from DWI, fMRI and MEG brain connectivity to extract an enriched description of the core-periphery structure in a group of AD patients and age- matched controls. Globally, the regional coreness - i.e., the probability of a region to be in the multiplex core - significantly decreased in AD patients as a result of the randomization process initiated by the neurodegeneration. Locally, the most impacted areas were in the core of the network - including temporal, parietal and occipital areas - while we reported compensatory increments for the peripheral regions in the sensorimotor system. Furthermore, these network changes significantly predicted the cognitive and memory impairment of patients. Taken together these results indicate that a more accurate description of neurodegenerative diseases can be obtained from the multimodal integration of neuroimaging-derived network data.

Introduction

The brain is a complex network where differently specialized areas are anatomically and functionally connected. Because of such interconnected structure, focal damages can affect the rest of the network through the interruption of communication pathways. Indeed, many neurological disorders affecting language, motor and sensory abilities are often due to a disconnection syndrome caused by the anatomical connectivity breakdown between the relevant brain areas (Schmahmann and Pandya, 2008; Geschwind, 1965). In the case of neurodegenerative diseases, the disconnection hypothesis is supported by a progressive death of neurons and synapses that induce gross atrophy. Empirical evidence has shown that Alzheimer's disease (AD) patients with severe motor and cognitive impairments exhibited anatomical disconnections among regions between cerebral hemispheres that resemble those observed in split-brain subjects (Delbeuck et al., 2007; Lakmache et al., 1998). In Parkinson's disease (PD) intrahemispheric dissociations between subcortical and cortical structures have been linked to disturbances in cognition, perception, emotion, and sleep (Cronin-Golomb, 2010). In addition, functional connectivity alterations within and between hemispheres have been reported in both AD (Blinowska et al., 2017; Sankari, 2010; Adler et al., 2003; Babiloni et al., 2009) and PD (Luo et al., 2015; Dubbelink et al., 2013) suggesting their potential role in the early diagnosis.

Altogether, these findings suggest that neurodegenerative diseases must be considered as a network problem. Recent approaches based on network theory have greatly advanced our understanding of the connection mechanisms characterizing brain diseases (Stam, 2014). Among others, decreased efficiency, modularity and hub centrality have been largely reported in neurodegeneration and associated with the stage of disease. Increasing evidence suggests that the core-periphery structure of the human connectome - supporting global integration of information among distant areas - is highly affected by the AD process and that resulting changes might be effective predictors of cognitive declines. On one hand, brain areas forming the core of the network - i.e. central and mutually connected nodes - have been reported to be preferentially attacked by AD (Yan et al., 2018). On the other hand, brain regions forming the periphery of the network - i.e. nodes that are only weakly connected to the other units in the network - appear to be crucial for the degeneration (Daianu et al., 2015). While these results refer to structural brain connectivity, the relative contribution of functional brain connectivity into the network core-periphery changes remain poorly understood.

Based on the aforementioned empirical and theoretical grounds, we hypothesize that neurodegeneration would affect the core-periphery structure of the brain network at both anatomical and functional levels. More specifically, we expected that the extraction of the core-periphery organization by integrating information from multimodal brain networks would give more accurate predictor of AD and cognitive impairment. Finally, based on the evidence that hubs are the most attacked nodes in many neurological diseases and psychiatric disorders (van den Heuvel and Sporns, 2013), we hypothesize that the core brain regions would be mostly impacted by the AD atrophy process.

To test these predictions, we considered multiple brain networks derived from DWI, fMRI and MEG data recorded in a group of AD patients and age-matched healthy controls (HC). Cognitive impairments in AD patients were described using multidomain behavioral measurements. We extracted the multimodal core-periphery structure of the brain networks through a multiplex network approach, where all the available information is kept at different connectivity layers. We evaluated how AD impacted the multiplex core-periphery organization and we tested the correlation of the regional coreness with the cognitive and memory impairment of patients. See Material and methods for more details on the experimental design and methods of analysis.

Results

Multimodal core of brain networks

We integrated multimodal information by constructing nine-layer multiplex brain networks containing DWI, fMRI and MEG connectivity between 68 cortical regions of interest (ROIs) (Material and methods). To estimate the likelihood of each ROI i to be in the multiplex core we computed its *coreness* C_i by counting how many times it was in the multiplex core across different density thresholds (Battiston et al., 2018). At each threshold, the

multiplex core-periphery structure was obtained by linearly combining the node strength of all the layers through a vector parameter c (Material and methods).

Because we do not know a-priori the best combination, we derived the optimal c^* by using a data-driven approach that efficiently explores the parameter space to maximize the difference between AD and HC regional coreness. Specifically, we used the particles swarm optimization algorithm (PSO) to maximize the Fisher's criterion $F(c)$ (Material and methods). Results show that the optimal c^* components are found to be highly heterogeneous and that the DWI layer, as well as MEG-alpha1 and fMRI layers, are the main contributors to separate the AD and HC group (Table 1, Figure 2a).

In the HC group, the multiplex core tended to include large portions of temporal, superior parietal and occipital cortices, and to a minor extent central and superior frontal regions (Figure 2b). On average AD patients exhibited a loss of coreness with respect to HC particularly in the temporal, superior parietal and occipital cortices. These regions were already known to form the core of multiplex brain networks derived from DTI and fMRI data (Battiston et al., 2018).

Reorganization of core-periphery structure in AD

To quantify the observed network changes we defined the coreness disruption index κ as the slope of the line obtained by regressing the difference between the average coreness (at each ROI and across subjects) of the two groups with the average coreness of the healthy one (Termenon et al., 2016) (Material and methods). We found a significant negative κ value indicating that AD preferentially attacks ROIs with a high coreness ($\kappa = -0.20, p = 2.45e-10$). This result was also consistent at the individual level when we extracted the coreness disruption index in each patient (Supplementary Table 1). In particular, by statistically comparing the average coreness of the two groups, we reported a significant decrease of coreness in core regions, such as temporal, parietal and occipital cortices as well as a significant increase of coreness in the right paracentral area which are instead more peripheral, ($p < 0.025$, Figure 3a,b, Supplementary Table 2).

Based on the hypothesis that AD is a disconnection syndrome (Geschwind, 1965; Delbeuck et al., 2003) leading to disorganized network configurations (Sanz-Arigita et al., 2010), we next generated a series of synthetic multiplex networks starting from the ones observed in the HC group and then progressively randomizing the same amount of links in each layer (Materials and methods). As expected the coreness disruption index decreased with the percentage of links that was randomly rewired. Notably, we could obtain the same significantly impacted κ values observed in the multiplex brain networks of the AD group ($p = 2.77e-4$) by rewiring between 45% and 60% of the links in the HC multiplex brain networks (Figure 4). Altogether, these findings indicate that the AD is associated with a pervasive random reconfiguration of structural and functional connectivity that primarily affects the nodes of the multiplex core.

Coreness disruption predicts cognitive and memory deficits

We finally conducted a correlation analysis to better understand how the observed multiplex brain network changes were associated with the behavioral performance of AD patients. Results show that both cognitive and memory deficits could be predicted by the individual loss of regional coreness. At the global scale, the coreness disruption index significantly correlated with the MMSE ($R = 0.46, p = 0.028$) as well as with the Immediate ($R = 0.47, p = 0.024$) and Free Recall ($R = 0.59, p = 0.005$) scores. The higher the κ values, the better was the performance of the patients (Figure 5a, Supplementary material). At the local scale, temporal, parietal and cortices were highly positively correlated with the behavior of patients. Notably, these ROIs overlapped with those exhibiting significant decreases of regional coreness with respect to healthy controls (Figure 3b). We found similar positive correlations for bilateral middle frontal ROIs ($R = 0.36, p = 0.092$ for left, $R = 0.35, p = 0.100$ for right), while areas in the motor-system appeared not to be involved except for the paracentral lobule that tended to negatively correlate with the MMSE ($R = -0.55, p = 0.007$) and Immediate Recall scores ($R = -0.36, p = 0.089$) scores (Figure 5b).

Discussion

Multiplex brain networks

The increasing availability of multimodal neuroimaging data holds a great potential to enrich our knowledge about fundamental neural mechanisms and to improve the precision of predictive biomarkers of brain diseases (Calhoun and Sui, 2016). However, how to integrate information from different neuroimaging modalities is still an open issue. Existing approaches have mainly focused on merging information at the level of the native data structure (e.g., signal or images) (Uludağ and Roebroek, 2014; Biessmann et al., 2011). Only recently, investigators have started to propose fusion algorithms in an effort to infer brain connectivity (Ng et al., 2012) or to detect mental states (Lei et al., 2011). Here, we adopted a complementary solution - based on the nascent field of multilayer network theory - which preserves the original nature of the different connectivity types. Similar approaches have been already used in the case of temporal (Betzel and Bassett, 2017; Domenico, 2017), multifrequency (Guillon et al., 2017; De Domenico et al., 2016) and DTI-fMRI brain networks (Battiston et al., 2017). This study considers for the first time brain networks obtained from three different neuroimaging modalities - DWI, fMRI and MEG - to construct multiplex brain networks consisting of nine connectivity layers and to derive an augmented description of their core-periphery structure in healthy and Alzheimer's diseased subjects. A crucial step in the multiplex construction is how to weight the different layers, which typically contain connectivity measured in units (e.g., number of fiber tracks and signal correlation) of different scales. While this is in general an arbitrary choice, here we established an objective way to associate a weight to each layer by maximizing the difference of regional coreness - i.e. the likelihood of each region to be in the core - between the groups. Results showed that all the three modalities are necessary to the group separation. In particular, for MEG only alpha1 was determinant while the other frequency layers had very low, or null, weights. This is in line with current evidence showing that alpha1 frequency band contains the most discriminant power and connectivity changes in AD (Babiloni et al., 2004b; Blinowska et al., 2017). Notably, DWI had a very high contribution coefficient as compared to the other layers. Core-periphery structure of diffusion-based networks is known to be very robust (van den Heuvel and Sporns, 2011; Hagmann et al., 2008) with respect to functional layers and this might possibly depend on the heterogeneity of the node degree distribution. Further research is needed to better understand how to normalize connectivity weights between layers when construction multiplex network construction.

Network reorganization in Alzheimer's disease

AD is associated with network changes affecting the structure and function of the brain at multiple spatial and temporal scales (Stam, 2014). It has been hypothesized that these network reconfigurations could result from disconnection patterns initiated by the gross atrophy of the brain. While several studies have found significant changes in terms of network efficiency, modularity and node centrality, the direction of these alterations - in terms of increments or decrements with respect to healthy controls - is often unclear and modality dependent (Tijms et al., 2013a). Here, we focused on the core-periphery structure of the human brain which has been shown to have a significant impact on cognition ensuring global integration across remote cortical areas (van den Heuvel and Sporns, 2011). Structural connectome studies have reported that AD patients, from the preclinical to dementia stages, have significant hub-concentrated lesion distributions (Crossley et al., 2014; Buckner et al., 2009; Dai et al., 2014; Brier et al., 2014; Shu et al., 2018). However, recent evidence is suggesting that network disruption is prevalent in the peripheral network components in both AD (Daianu et al., 2015) and mild cognitive impairment (MCI) patients (Zhao et al., 2017). These inconsistent findings suggest that the network disruption mechanisms remain unclear. By integrating information from structural and functional brain networks we aimed to overcome this controversy and provide a more comprehensive insight. Our multiplex network approach shows that core regions were globally affected in AD patients as compared to HC subjects and that this result could be modeled by a global random rewiring process. Specifically, we reported significant decrements of coreness in temporal and parietal cortices, which are heavily affected by atrophy processes and beta-amyloid deposition (Buckner et al., 2008). However, this change was paralleled by a significant increase of coreness in the paracentral lobules, which originally belonged to the multiplex periphery. Because regions of the sensorimotor system -

such as paracentral lobule - are not directly affected by the atrophy process (Agosta et al., 2010), we speculate that possible compensatory mechanisms could have therefore taken place. In line with this hypothesis, recent findings suggest that more efficient motor commands in mild cognitive impaired patients could trigger the later functional decline (Kubicki et al., 2016). Longitudinal studies involving healthy subjects converting into AD will be fundamental to confirm or reject this prediction (Dubois et al., 2016).

Connectivity-based biomarkers of clinical behavior

Brain wiring organization is critically associated with human cognition, behavior as well as with several neurological and psychiatric disorders (Stam, 2014). Network indices describing core-periphery and rich-club organization in structural brain networks have been shown to predict cognitive and motor deficits in multiple sclerosis (Stellmann et al., 2017), and Huntington disease (Harrington et al., 2015), as well as communication impairment in schizophrenia (van den Heuvel et al., 2013). More pertinent to this work, rich-club biomarkers extracted from DTI networks have been shown to correlate with cognitive and memory deficits in Alzheimer’s disease (Daianu et al., 2015; Tijms et al., 2013b; Stam et al., 2009).

Here, we showed that the coreness disruption index - quantifying the global tendency to weaken core-periphery structure in multimodal brain networks - determined the cognitive and memory performance of our AD patients. Patients with a stronger core-periphery organization had better MMSE and FSCRT scores. At the local scale, temporal, parietal as well as frontal areas tended to positively correlate with patient’s behavior. These association regions have been shown to be implicated in the prediction of AD cognitive performance (Khachiyants and Kim, 2012) and more in general in memory and language (Squire, 1992; Gordon, 1995; Pochon et al., 2002). We also found negative correlations with the paracentral lobule (especially right), a region that is typically involved in motor-related tasks but not in integrative functions.

From a network perspective, the coreness of regions that tended to be in the multiplex core - such as temporal, parietal and occipital cortices - were positively correlated with patients’ performance, while among the peripheral areas the paracentral lobule was negatively correlated with the behavior. This means that in presence of more severe cognitive and memory deficits the relative decrease of connectivity in core regions tended to be replaced by periphery components of the brain system. This result would confirm the existence of an adjusting mechanism, where the sensorimotor system might be involved in the compensation of connectivity loss in systems that are directly impacted by Amyloid-beta plaques and tau neurofibrillary tangles accumulation (Iaccarino et al., 2018).

Methodological considerations

The basic algorithm behind the detection of the core-periphery structure in multiplex networks is purely deterministic (Ma and Mondragón, 2015). This means that in principle we could not evaluate the statistical relevance of the identified structure. To overcome this limitation, we adopted a procedure that consisted in extracting the core-periphery structure from a series of multiplex networks obtained by filtering the actual brain multiplex network with increasing density thresholds (Battiston et al., 2018). This way we could derive a probabilistic measure of coreness by counting how many times each ROI was assigned to the core across all the possible thresholds. For the sake of simplicity we filtered each brain multiplex by retaining the strongest links so that the average node degree of each layer ranged from $k = 1$ to $k = N - 1$ (Materials and methods).

After filtering we did not binarize the surviving links so that we applied the core-periphery algorithm to sparse weighted multiplex networks. This approach allows us to exploit all the available information in the multiplex brain networks. At the same time, we remark that additional care is needed, as it introduces issues related to the different nature and distributions of the link weights (Buldú and Papo, 2018). Here, we mitigated this problem by using in the core-periphery algorithm the vector c of parameters that can weight the contribution of each layer (Material and methods). Alternative solutions have been recently proposed taking into account the normalization of the weight across the layers by means of singular value decomposition (Mandke et al., 2018).

We used an optimization algorithm - namely the particle swarm optimization - to find the best combination of c components that maximized the difference of the coreness between AD and HC subjects (Material and methods). This method presents two limitations that are important to mention here. First, the time complexity increases exponentially with the number of layers M in order to find a stable solution. We verified that for $M > 10$ the research complexity becomes rapidly intractable due to the large space of parameter combination to explore. Second, the cost function optimized by the algorithm and used to evaluate how segregated the two groups are (i.e. two sets of coreness vectors) should be carefully chosen as its accuracy is highly impacted by the size of the feature space (here N , the number of ROIs) and the size of the samples (here the size of the cohorts). More advanced techniques taking into account the possible nonlinear and/or non-Euclidean nature of the feature space should be considered for very large networks (e.g., support vector machines, Riemannian geometry).

Conclusion

Consistent with our hypothesis, we have shown that AD atrophy process generates multimodal connectivity changes that can be quantified by a multilayer network approach. Specifically we have identified that both core and - to a minor extent - peripheral cortical areas are affected in AD, and that the direction of the effect was opposite. Decrease of coreness in temporal, parietal and occipital areas - forming the rich core of the human brain - is paralleled by a possible compensatory increment in cortical regions that are in the sensorimotor system and that are more peripheral. These cortical network signatures varied over individuals and were significant predictors of cognitive and memory deficits. Furthermore, we reported a general framework for the statistical comparison of core-periphery organization in arbitrary multiplex networks. Taken together, our results offer new insights into the crucial role of core-periphery organization in neurodegenerative diseases.

Material and methods

Cohort inclusion

The study involved 23 Alzheimer's diseased (AD) patients (13 women) and 26 healthy age-matched control (HC) subjects (19 women). All participants underwent the Mini-Mental State Examination (MMSE) for global cognition and the Free and Cued Selective Reminding Test (FCSRT) for verbal episodic memory. Inclusion criteria for all participants were: *i*) age between 50 and 90; *ii*) absence of general evolutive pathology; *iii*) no previous history of psychiatric diseases; *iv*) no contraindication to MRI examination; *v*) French as a mother tongue. Specific criteria for AD patients were: *i*) clinical diagnosis of Alzheimer's disease; *ii*) Mini-Mental State Examination (MMSE) score greater or equal to 18. All subjects gave written informed consent for participation in the study, which was approved by the local ethics committee of the Pitie-Salpetriere Hospital. All experiments were performed in accordance with relevant guidelines and regulation.

Data acquisition and pre-processing

Magnetic resonance imaging (MRI) acquisitions were obtained using a 3T system (Siemens Trio, 32-channel system, with a 12-channel head coil). The MRI examination included: *(i)* 3D T1-weighted volumetric magnetization-prepared rapid gradient echo (MPRAGE) sequence with the following parameters: thickness = 1 mm isotropic, repetition time (TR) = 2300 ms, echo time (TE) = 4.18 ms, inversion time (TI) = 900 ms, acquisition matrix = 256×256 ; *(ii)* echo planar imaging (EPI) sequence with the following parameters: one image with no diffusion sensitization (b0 image) and 50 diffusion-weighted images (DWI) at $b = 1500 \text{ s/mm}^2$, thickness = 2 mm isotropic, TR = 13000 ms, TE = 92 ms, flip angle = 90° , acquisition matrix = 128×116 ; *(iii)* functional MRI (fMRI) resting-state sequence sensitive to blood oxygenation level-dependent (BOLD) contrast with

the following parameters: 200 images, thickness = 3 mm isotropic, TR = 2400 ms, TE = 30 ms, flip angle = 90°, acquisition matrix = 64 × 64. All MR images were processed using the Clinica software (<http://www.clinica.run>). We first used the `t1-freesurfer-cross-sectional` pipeline to process T1-weighted images. This pipeline is a wrapper of different tools of the FreeSurfer software (<http://surfer.nmr.mgh.harvard.edu/>) (Fischl, 2012). It includes segmentation of subcortical structures, extraction of cortical surfaces, cortical thickness estimation, spatial normalization onto the FreeSurfer surface template (FsAverage), and parcellation of cortical regions. Functional MRI images pre-processing have been conducted using the `fmri-preprocessing` pipeline. Slice timing correction, head motion correction and unwarping have been applied using SPM12 tools (www.fil.ion.ucl.ac.uk/spm). Separately the brain mask has been extracted from the T1 image of each subject using FreeSurfer. The resulting fMRI images have then been registered to the brain-masked T1 image of each subject using SPM's registration tool. Finally, diffusion-weighted images have been processed using the `dwi-preprocessing` pipeline of Clinica. For each subject, all raw DWI volumes were rigidly registered (6 degrees of freedom (dof)) to the reference b0 image (DWI volume with no diffusion sensitization) to correct for head motion. The diffusion weighting directions were appropriately updated (Leemans and Jones, 2009). An affine registration (12 dof) was then performed between each DWI volume and the reference b0 to correct for eddy current distortions. These registrations were done using the FSL flirt tool (www.fmrib.ox.ac.uk/fsl). To correct for echo-planar imaging (EPI) induced susceptibility artifacts, the field map image was used as proposed by (Jezzard and Balaban, 1995) with the FSL prelude/fugue tools. Finally, the DWI volumes were corrected for nonuniform intensity using the ANTs N4 bias correction algorithm (Tustison et al., 2010). A single multiplicative bias field from the reference b0 image was estimated, as suggested in (Jeurissen et al., 2014).

The magnetoencephalography (MEG) experimental protocol consisted in a resting-state with eyes-closed (EC). Subjects seated comfortably in a dimly lit electromagnetically and acoustically shielded room and were asked to relax. MEG signals were collected using a whole-head MEG system with 102 magnetometers and 204 planar gradiometers (Elekta Neuromag TRIUX MEG system) at a sampling rate of 1000 Hz and on-line low-pass filtered at 330 Hz. The ground electrode was located on the right shoulder blade. An electrocardiogram (EKG, Ag/AgCl electrodes) was placed on the left abdomen for artifacts correction and a vertical electrooculogram (EOG) was simultaneously recorded. Four small coils were attached to the participant in order to monitor head position and to provide co-registration with the anatomical MRI. The physical landmarks (the nasion, the left and right pre-auricular points) were digitized using a Polhemus Fastrak digitizer (Polhemus, Colchester, VT). We extracted three consecutive clean epochs of approximately 2 minutes each.

Signal space separation was performed using `MaxFilter` to remove external noise. We used in-house software to remove cardiac and ocular blink artifacts from MEG signals by means of principal component analysis. We visually inspected the preprocessed MEG signals in order to remove epochs that still presented spurious contamination. At the end of the process, we obtained a coherent dataset consisting of three clean preprocessed epochs per subject. We reconstructed the MEG activity on the cortical surface by using a source imaging technique (He, 1999; Baillet et al., 2001): *i*) We used the previously segmented T1-weighted images of each single subject (Fischl et al., 2002, 2004) to import cortical surfaces in the Brainstorm software (Tadel et al., 2011) where they were modeled with approximately 20000 equivalent current dipoles (i.e., the vertices of the cortical meshes). *ii*) We applied the wMNE (weighted Minimum Norm Estimate) algorithm with overlapping spheres (Lin et al., 2006) to solve the linear inverse problem. Both magnetometer and gradiometer, whose position has been registered on the T1 image using the digitized head points, were used to localize the activity over the cortical surface.

Construction of brain networks

We built, for each modality, one or multiple brain connectivity networks whose nodes are regions of interests (ROIs) defined by the Desikan cortical atlas parcellation (Desikan et al., 2006) ($N = 68$ regions); and links are weighted by a given connectivity measure estimated between each pair of nodes resulting in 68×68 fully symmetric adjacency matrices.

In the case of MEG, we used the spectral coherence as a connectivity estimator with the following parameters: window length = 2 s, window type = sliding Hanning, overlap = 25% number of FFT points (NFFT) = 2000 for a frequency resolution of 0.5 Hz between 2 Hz and 45 Hz included.

We then averaged the connectivity matrices within the following characteristic frequency bands (Stam et al., 2002; Babiloni et al., 2004a): *delta* (2–4 Hz), *theta* (4.5–7.5 Hz), *alpha1* (8–10.5 Hz), *alpha2* (11–13 Hz), *beta1* (13.5–20 Hz), *beta2* (20.5–29.5 Hz) and *gamma* (30–45 Hz). We finally averaged the connectivity matrices across the three available epochs to obtain a robust estimate of the individual brain networks.

For fMRI data, we focused our analysis on the scale 2 wavelet correlation matrices that represented - with a TR = 2400ms - the functional connectivity in the frequency interval 0.05–0.10Hz (Biswal et al., 1995; Cordes et al., 2001; Achard, 2006).

For DWI data, we used the Clinica software to estimate the fiber orientation distributions (FODs) using constrained spherical deconvolution (CSD) algorithm from MRtrix3 `dwi2fod` tool and tractography based on iFOD2 algorithm from MRtrix3 `tckgen` tool. The connectome is finally estimated by counting the number of tracts connecting each pair of nodes according to the given parcellation file using MRtrix3 `tck2connectome` tool.

Network methods and models

We constructed multiplex brain networks in each subject by spatially aligning DWI, fMRI and MEG source reconstructed connectivity networks. This led to the following multiplex network with $M = 9$ layers:

$$\mathcal{M} = \{W^{[m]}, \forall m \in \{\text{MEG}_\delta, \dots, \text{MEG}_\gamma, \text{fMRI}, \text{DWI}\}\},$$

where $W^{[m]} = \{w_{ij}^{[m]}\}$ is the connectivity matrix containing the weights of the connections between the ROIs i and j in the modality m .

To extract the coreness of the nodes from the resulting multiplex networks, we followed the procedure described by Battiston et al. (2018). First, we filtered each layer by preserving the strongest weights for a broad range of increasing thresholds. Specifically, we considered density-based thresholds so that each layer had the same average node degree from $k = 1$ to $k = N - 1$. Then, for each threshold we computed the core-periphery of the filtered multiplex network by evaluating (i) the multiplex richness μ_i of node i , defined as follows:

$$\mu_i = \sum_{m=1}^M c^{[m]} s_i^{[m]},$$

with $s_i^{[m]}$ the strength of the node in the m -th layer, and $c^{[m]}$ the components of the vector c that modulate the contribution of each modality-specific layer. And (ii), similarly to the original paper, we decomposed the richness function into two components based on the links of node i that are going towards nodes with lower richness and those towards nodes with higher richness $s^{[m]} = s^{[m]-} + s^{[m]+}$. Thus, the multiplex richness of a node towards richer nodes is defined as follows:

$$\mu_i^+ = \sum_{m=1}^M c^{[m]} s_i^{[m]+}.$$

We finally counted the number of times that each node was in the core across all the explored thresholds and we normalized by the maximum theoretical value. As a result, we obtained the coreness C_i that can be written as follow:

$$C_i = \frac{1}{N-1} \sum_{k=1}^{N-1} \delta_i^{[k]},$$

where

$$\delta_i^{[k]} = \begin{cases} 1, & \text{if node } i \text{ is in the core for the average node degree } k. \\ 0, & \text{otherwise.} \end{cases}$$

We generated random multiplex networks by shuffling a given percentage of links separately in each layer starting from the actual multiplex brain network of the HC group. This way the weight distribution was unchanged and only the topology of the network is impacted. Specifically, for each HC individual, we generated n_{rand} new randomized multiplexes. We chose the minimum number of randomizations necessary to obtain a variance approximatively equal to the one observed in the HC and AD groups. This number was $n_{\text{rand}} = 3$ and gave in total $N_{\text{RA}} = n_{\text{rand}} \times N_{\text{HC}} = 78$ samples.

Particles swarm optimization and statistical analysis

We used the PSO algorithm (Kennedy and Eberhart, 1995) under the MATLAB(R) software with the default parameters. The Fisher's criterion $F(c)$ was defined as follow:

$$F(c) = \frac{(\bar{I}_{\text{AD}}(c) - \bar{I}_{\text{HC}}(c))^2}{s_{\text{AD}}^2 + s_{\text{HC}}^2},$$

with $\bar{I}_{\text{Pop}}(c)$, the average local (i.e. node level) index, here the coreness \mathcal{C} , over a population Pop, which in our case belongs to $\{\text{AD}, \text{HC}\}$, and,

$$s_{\text{Pop}}^2 = \sum_{s \in \text{Pop}} (I_s(c) - \bar{I}_{\text{Pop}}(c))^2,$$

with s a subject belonging the population Pop.

Since, in our case, $F(c) = F(ac), \forall a \in \mathbb{R}^+$, and in order to save one dimension in the searching space, we expressed the coefficient c as a point on the positive section of the unitary hypersphere of dimension $M = 9$ such that:

$$c = \begin{pmatrix} \sin \phi_1 \dots \sin \phi_8 \\ \sin \phi_1 \dots \sin \phi_7 \cos \phi_8 \\ \sin \phi_1 \dots \sin \phi_6 \cos \phi_7 \\ \sin \phi_1 \dots \sin \phi_5 \cos \phi_6 \\ \sin \phi_1 \dots \sin \phi_4 \cos \phi_5 \\ \sin \phi_1 \dots \sin \phi_3 \cos \phi_4 \\ \sin \phi_1 \sin \phi_2 \cos \phi_3 \\ \sin \phi_1 \cos \phi_2 \\ \cos \phi_1 \end{pmatrix}, \phi_k \in \left[0, \frac{\pi}{2}\right], \forall k \in [1, M-1].$$

To consider the non-gaussian nature of the data we considered non-parametric statistics when assessing differences between populations and prediction of behavioral scores. To these ends, we used respectively permutation t-tests and Spearman correlation coefficients. The statistical thresholds were set to $\alpha = 0.05$ and we applied a rough false discovery rate (FDR) correction to account for the $N = 68$ post-hoc tests at the level of brain regions ($\alpha_{\text{FDR}} = 0.025$).

Acknowledgements

The research leading to these results has received funding from the program “Investissements d’avenir” ANR-10-IAIHU-06 (Agence Nationale de la Recherche-10-IA Institut Hospitalo-Universitaire-6), ANR-11-IDEX-004 (Agence Nationale de la Recherche-11- Initiative d’Excellence-004, project LearnPETMR number SU-16-R-EMR-16) and from Agence Nationale de la Recherche (project HM-TC, grant number ANR-09-EMER-006). FD acknowledges support from the “Agence Nationale de la Recherche” through contract number ANR-15-NEUC-0006-02. The content is solely the responsibility of the authors and does not necessarily represent the official views of any of the funding agencies.

References

- S. Achard. A Resilient Low-Frequency, Small-World Human Brain Functional Network with Highly Connected Association Cortical Hubs. *Journal of Neuroscience*, 26(1):63–72, jan 2006. doi: 10.1523/jneurosci.3874-05.2006. URL <https://doi.org/10.1523%2Fjneurosci.3874-05.2006>.
- G. Adler, S. Brassens, and A. Jajcevic. EEG coherence in Alzheimer’s dementia. *Journal of Neural Transmission*, 110(9):1051–1058, sep 2003. doi: 10.1007/s00702-003-0024-8. URL <https://doi.org/10.1007%2Fs00702-003-0024-8>.
- F Agosta, MA Rocca, E Pagani, M Absinta, G Magnani, A Marcone, M Falautano, G Comi, ML Gorno-Tempini, and M Filippi. Sensorimotor network rewiring in mild cognitive impairment and Alzheimer’s disease. *Hum Brain Mapp*, 31:515–25, Apr 2010.
- Claudio Babiloni, Raffaele Ferri, Davide V. Moretti, Andrea Strambi, Giuliano Binetti, Gloria Dal Forno, Florinda Ferreri, Bartolo Lanuzza, Claudio Bonato, Flavio Nobili, Guido Rodriguez, Serenella Salinari, Stefano Passero, Raffaele Rocchi, C. J. Stam, and Paolo M. Rossini. Abnormal fronto-parietal coupling of brain rhythms in mild Alzheimer’s disease: a multicentric EEG study. *Eur. J. Neurosci.*, 19(9):2583–2590, may 2004a. ISSN 0953-816X. doi: 10.1111/j.0953-816X.2004.03333.x.
- Claudio Babiloni, Raffaele Ferri, Davide V. Moretti, Andrea Strambi, Giuliano Binetti, Gloria Dal Forno, Florinda Ferreri, Bartolo Lanuzza, Claudio Bonato, Flavio Nobili, Guido Rodriguez, Serenella Salinari, Stefano Passero, Raffaele Rocchi, C. J. Stam, and Paolo M. Rossini. Abnormal fronto-parietal coupling of brain rhythms in mild Alzheimer’s disease: a multicentric EEG study. *European Journal of Neuroscience*, 19(9):2583–2590, may 2004b. doi: 10.1111/j.0953-816x.2004.03333.x. URL <https://doi.org/10.1111%2Fj.0953-816x.2004.03333.x>.
- Claudio Babiloni, Raffaele Ferri, Giuliano Binetti, Fabrizio Vecchio, Giovanni B. Frisoni, Bartolo Lanuzza, Carlo Miniussi, Flavio Nobili, Guido Rodriguez, Francesco Rundo, Andrea Cassarino, Francesco Infarinato, Emanuele Cassetta, Serenella Salinari, Fabrizio Eusebi, and Paolo M. Rossini. Directionality of EEG synchronization in Alzheimer’s disease subjects. *Neurobiology of Aging*, 30(1):93–102, jan 2009. doi: 10.1016/j.neurobiolaging.2007.05.007. URL <https://doi.org/10.1016%2Fj.neurobiolaging.2007.05.007>.
- S. Baillet, J. J. Riera, G. Marin, J. F. Mangin, J. Aubert, and L. Garnero. Evaluation of inverse methods and head models for EEG source localization using a human skull phantom. *Phys Med Biol*, 46(1):77–96, jan 2001. ISSN 0031-9155.
- Federico Battiston, Vincenzo Nicosia, Mario Chavez, and Vito Latora. Multilayer motif analysis of brain networks. *Chaos: An Interdisciplinary Journal of Nonlinear Science*, 27(4):047404, apr 2017. doi: 10.1063/1.4979282. URL <https://doi.org/10.1063%2F1.4979282>.

- Federico Battiston, Jeremy Guillon, Mario Chavez, Vito Latora, and Fabrizio De Vico Fallani. Multiplex core–periphery organization of the human connectome. *Journal of The Royal Society Interface*, 15(146): 20180514, sep 2018. doi: 10.1098/rsif.2018.0514. URL <https://doi.org/10.1098/rsif.2018.0514>.
- Richard F. Betzel and Danielle S. Bassett. Multi-scale brain networks. *NeuroImage*, 160:73–83, oct 2017. doi: 10.1016/j.neuroimage.2016.11.006. URL <https://doi.org/10.1016/j.neuroimage.2016.11.006>.
- Felix Biessmann, Sergey Plis, Frank C. Meinecke, Tom Eichele, and Klaus-Robert Muller. Analysis of Multimodal Neuroimaging Data. *IEEE Reviews in Biomedical Engineering*, 4:26–58, 2011. doi: 10.1109/rbme.2011.2170675. URL <https://doi.org/10.1109/rbme.2011.2170675>.
- Bharat Biswal, F. Zerrin Yetkin, Victor M. Haughton, and James S. Hyde. Functional connectivity in the motor cortex of resting human brain using echo-planar mri. *Magnetic Resonance in Medicine*, 34(4):537–541, oct 1995. doi: 10.1002/mrm.1910340409. URL <https://doi.org/10.1002/mrm.1910340409>.
- Katarzyna J. Blinowska, Franciszek Rakowski, Maciej Kaminski, Fabrizio De Vico Fallani, Claudio Del Percio, Roberta Lizio, and Claudio Babiloni. Functional and effective brain connectivity for discrimination between Alzheimer’s patients and healthy individuals: A study on resting state EEG rhythms. *Clinical Neurophysiology*, 128(4):667–680, apr 2017. doi: 10.1016/j.clinph.2016.10.002. URL <https://doi.org/10.1016/j.clinph.2016.10.002>.
- Matthew R. Brier, Jewell B. Thomas, Anne M. Fagan, Jason Hassenstab, David M. Holtzman, Tammie L. Benzinger, John C. Morris, and Beau M. Ances. Functional connectivity and graph theory in preclinical Alzheimer’s disease. *Neurobiology of Aging*, 35(4):757–768, apr 2014. doi: 10.1016/j.neurobiolaging.2013.10.081. URL <https://doi.org/10.1016/j.neurobiolaging.2013.10.081>.
- R. L. Buckner, J. Sepulcre, T. Talukdar, F. M. Krienen, H. Liu, T. Hedden, J. R. Andrews-Hanna, R. A. Sperling, and K. A. Johnson. Cortical Hubs Revealed by Intrinsic Functional Connectivity: Mapping Assessment of Stability, and Relation to Alzheimer’s Disease. *Journal of Neuroscience*, 29(6):1860–1873, feb 2009. doi: 10.1523/jneurosci.5062-08.2009. URL <https://doi.org/10.1523/jneurosci.5062-08.2009>.
- Randy L. Buckner, Jessica R. Andrews-Hanna, and Daniel L. Schacter. The Brain’s Default Network. *Annals of the New York Academy of Sciences*, 1124(1):1–38, mar 2008. doi: 10.1196/annals.1440.011. URL <https://doi.org/10.1196/annals.1440.011>.
- Javier M. Buldú and David Papo. Can multilayer brain networks be a real step forward? *Physics of Life Reviews*, 24:153–155, mar 2018. doi: 10.1016/j.plrev.2017.12.007. URL <https://doi.org/10.1016/j.plrev.2017.12.007>.
- Vince D. Calhoun and Jing Sui. Multimodal Fusion of Brain Imaging Data: A Key to Finding the Missing Link(s) in Complex Mental Illness. *Biological Psychiatry: Cognitive Neuroscience and Neuroimaging*, 1(3):230–244, may 2016. doi: 10.1016/j.bpsc.2015.12.005. URL <https://doi.org/10.1016/j.bpsc.2015.12.005>.
- D Cordes, VM Haughton, K Arfanakis, JD Carew, PA Turski, CH Moritz, MA Quigley, and ME Meyerand. Frequencies contributing to functional connectivity in the cerebral cortex in resting-state data. *AJNR Am J Neuroradiol*, 22:1326–33, Aug 2001.
- Alice Cronin-Golomb. Parkinson’s Disease as a Disconnection Syndrome. *Neuropsychology Review*, 20(2):191–208, apr 2010. doi: 10.1007/s11065-010-9128-8. URL <https://doi.org/10.1007/s11065-010-9128-8>.
- Nicolas A. Crossley, Andrea Mechelli, Jessica Scott, Francesco Carletti, Peter T. Fox, Philip McGuire, and Edward T. Bullmore. The hubs of the human connectome are generally implicated in the anatomy of brain disorders. *Brain*, 137(8):2382–2395, jun 2014. doi: 10.1093/brain/awu132. URL <https://doi.org/10.1093/brain/awu132>.
- Zhengjia Dai, Chaogan Yan, Kuncheng Li, Zhiqun Wang, Jinhui Wang, Miao Cao, Qixiang Lin, Ni Shu, Mingrui Xia, Yanchao Bi, and Yong He. Identifying and Mapping Connectivity Patterns of Brain Network Hubs in

- Alzheimer's Disease. *Cerebral Cortex*, 25(10):3723–3742, oct 2014. doi: 10.1093/cercor/bhu246. URL <https://doi.org/10.1093%2Fcercor%2Fbhu246>.
- Madelaine Daianu, Neda Jahanshad, Talia M. Nir, Clifford R. Jack, Michael W. Weiner, Matt A. Bernstein, and Paul M. Thompson and. Rich club analysis in the Alzheimer's disease connectome reveals a relatively undisturbed structural core network. *Human Brain Mapping*, 36(8):3087–3103, jun 2015. doi: 10.1002/hbm.22830. URL <https://doi.org/10.1002%2Fhbm.22830>.
- Manlio De Domenico, Shuntaro Sasai, and Alex Arenas. Mapping multiplex hubs in human functional brain network. *arXiv:1603.05897 [cond-mat, physics:physics, q-bio]*, mar 2016. URL <http://arxiv.org/abs/1603.05897>. arXiv: 1603.05897.
- X. Delbeuck, M. Van der Linden, and F. Collette. Alzheimer's disease as a disconnection syndrome? *Neuropsychol Rev*, 13(2):79–92, jun 2003. ISSN 1040-7308.
- X. Delbeuck, F. Collette, and M. Van der Linden. Is Alzheimer's disease a disconnection syndrome? *Neuropsychologia*, 45(14):3315–3323, jan 2007. doi: 10.1016/j.neuropsychologia.2007.05.001. URL <https://doi.org/10.1016%2Fj.neuropsychologia.2007.05.001>.
- Rahul S. Desikan, Florent Ségonne, Bruce Fischl, Brian T. Quinn, Bradford C. Dickerson, Deborah Blacker, Randy L. Buckner, Anders M. Dale, R. Paul Maguire, Bradley T. Hyman, Marilyn S. Albert, and Ronald J. Killiany. An automated labeling system for subdividing the human cerebral cortex on MRI scans into gyral based regions of interest. *NeuroImage*, 31(3):968–980, jul 2006. doi: 10.1016/j.neuroimage.2006.01.021. URL <https://doi.org/10.1016%2Fj.neuroimage.2006.01.021>.
- Manlio De Domenico. Multilayer modeling and analysis of human brain networks. *GigaScience*, 6(5), feb 2017. doi: 10.1093/gigascience/gix004. URL <https://doi.org/10.1093%2Fgigascience%2Fgix004>.
- Kim T. E. Olde Dubbelink, Arjan Hillebrand, Diederick Stoffers, Jan Berend Deijen, Jos W. R. Twisk, Cornelis J. Stam, and Henk W. Berendse. Disrupted brain network topology in Parkinson's disease: a longitudinal magnetoencephalography study. *Brain*, 137(1):197–207, nov 2013. doi: 10.1093/brain/awt316. URL <https://doi.org/10.1093%2Fbrain%2Fawt316>.
- Bruno Dubois, Harald Hampel, Hova Bakardjian, Francis Nyasse, Simone Lista, Foudil Lamari, Marie-Claude Potier, Olivier Colliot, Habib Benali, Stéphane Epelbaum, and Marie-Odile Habert. INSIGHT-AD STUDY: A MONOCENTRIC COHORT FOR THE STUDY OF THE PRECLINICAL STAGE OF ALZHEIMER'S DISEASE. *Alzheimer's & Dementia*, 12(7):P335, jul 2016. doi: 10.1016/j.jalz.2016.06.614. URL <https://doi.org/10.1016%2Fj.jalz.2016.06.614>.
- Bruce Fischl. FreeSurfer. *NeuroImage*, 62(2):774–781, aug 2012. doi: 10.1016/j.neuroimage.2012.01.021. URL <https://doi.org/10.1016%2Fj.neuroimage.2012.01.021>.
- Bruce Fischl, David H. Salat, Evelina Busa, Marilyn Albert, Megan Dieterich, Christian Haselgrove, Andre van der Kouwe, Ron Killiany, David Kennedy, Shuna Klaveness, Albert Montillo, Nikos Makris, Bruce Rosen, and Anders M. Dale. Whole brain segmentation: automated labeling of neuroanatomical structures in the human brain. *Neuron*, 33(3):341–355, jan 2002. ISSN 0896-6273.
- Bruce Fischl, David H. Salat, Andr  J. W. van der Kouwe, Nikos Makris, Florent S gonne, Brian T. Quinn, and Anders M. Dale. Sequence-independent segmentation of magnetic resonance images. *Neuroimage*, 23 Suppl 1:569–84, 2004. ISSN 1053-8119. doi: 10.1016/j.neuroimage.2004.07.016.
- Norman Geschwind. DISCONNEXION SYNDROMES IN ANIMALS AND MAN. *Brain*, 88(2):237–237, June 1965. ISSN 0006-8950. doi: 10.1093/brain/88.2.237. URL <https://academic.oup.com/brain/article/88/2/237/259098>.
- Barry Gordon. Memory amnesia, and the hippocampal system. *Electroencephalography and Clinical Neurophysiology*, 95(6):479, dec 1995. doi: 10.1016/0013-4694(95)90026-8. URL <https://doi.org/10.1016%2F0013-4694%2895%2990026-8>.

- J. Guillon, Y. Attal, O. Colliot, V. La Corte, B. Dubois, D. Schwartz, M. Chavez, and F. De Vico Fallani. Loss of brain inter-frequency hubs in Alzheimer's disease. *Scientific Reports*, 7(1), sep 2017. doi: 10.1038/s41598-017-07846-w. URL <https://doi.org/10.1038/s41598-017-07846-w>.
- Patric Hagmann, Leila Cammoun, Xavier Gigandet, Reto Meuli, Christopher J Honey, Van J Wedeen, and Olaf Sporns. Mapping the Structural Core of Human Cerebral Cortex. *PLoS Biology*, 6(7):e159, jul 2008. doi: 10.1371/journal.pbio.0060159. URL <https://doi.org/10.1371/journal.pbio.0060159>.
- Deborah L. Harrington, Mikail Rubinov, Sally Durgerian, Lyla Mourany, Christine Reece, Katherine Koenig, Ed Bullmore, Jeffrey D. Long, Jane S. Paulsen, and Stephen M. Rao and. Network topology and functional connectivity disturbances precede the onset of Huntington's disease. *Brain*, 138(8):2332–2346, jun 2015. doi: 10.1093/brain/awv145. URL <https://doi.org/10.1093/brain/awv145>.
- B. He. Brain electric source imaging: scalp Laplacian mapping and cortical imaging. *Crit Rev Biomed Eng*, 27(3-5):149–188, 1999. ISSN 0278-940X.
- L Iaccarino, G Tammewar, N Ayakta, SL Baker, A Bejanin, AL Boxer, ML Gorno-Tempini, M Janabi, JH Kramer, A Lazaris, SN Lockhart, BL Miller, ZA Miller, JP O'Neil, R Ossenkoppele, HJ Rosen, DR Schonhaut, WJ Jagust, and GD Rabinovici. Local and distant relationships between amyloid, tau and neurodegeneration in Alzheimer's Disease. *Neuroimage Clin*, 17:452–464, 2018.
- Ben Jeurissen, Jacques-Donald Tournier, Thijs Dhollander, Alan Connelly, and Jan Sijbers. Multi-tissue constrained spherical deconvolution for improved analysis of multi-shell diffusion MRI data. *NeuroImage*, 103:411–426, dec 2014. doi: 10.1016/j.neuroimage.2014.07.061. URL <https://doi.org/10.1016/j.neuroimage.2014.07.061>.
- Peter Jezzard and Robert S. Balaban. Correction for geometric distortion in echo planar images from B0 field variations. *Magnetic Resonance in Medicine*, 34(1):65–73, jul 1995. doi: 10.1002/mrm.1910340111. URL <https://doi.org/10.1002/mrm.1910340111>.
- J. Kennedy and R. Eberhart. Particle swarm optimization. In *Proceedings of ICNN'95 - International Conference on Neural Networks*. IEEE, 1995. doi: 10.1109/icnn.1995.488968. URL <https://doi.org/10.1109/icnn.1995.488968>.
- Nina Khachiyants and Kye Y. Kim. Mini-mental status exam mapping to the corresponding brain areas in dementia. *Applied Technologies and Innovations*, 7(2):55–58, jun 2012. doi: 10.15208/ati.2012.7. URL <https://doi.org/10.15208/ati.2012.7>.
- Alexandre Kubicki, Lilian Fautrelle, Julien Bourrelier, Olivier Rouaud, and France Mourey. The Early Indicators of Functional Decrease in Mild Cognitive Impairment. *Frontiers in Aging Neuroscience*, 8, aug 2016. doi: 10.3389/fnagi.2016.00193. URL <https://doi.org/10.3389/fnagi.2016.00193>.
- Y. Lakmache, M. Lassonde, S. Gauthier, J.-Y. Frigon, and F. Lepore. Interhemispheric disconnection syndrome in Alzheimer's disease. *Proceedings of the National Academy of Sciences*, 95(15):9042–9046, jul 1998. doi: 10.1073/pnas.95.15.9042. URL <https://doi.org/10.1073/pnas.95.15.9042>.
- Alexander Leemans and Derek K. Jones. TheB-matrix must be rotated when correcting for subject motion in DTI data. *Magnetic Resonance in Medicine*, 61(6):1336–1349, jun 2009. doi: 10.1002/mrm.21890. URL <https://doi.org/10.1002/mrm.21890>.
- Xu Lei, Dirk Ostwald, Jiehui Hu, Chuan Qiu, Camillo Porcaro, Andrew P. Bagshaw, and Dezhong Yao. Multimodal Functional Network Connectivity: An EEG-fMRI Fusion in Network Space. *PLoS ONE*, 6(9):e24642, sep 2011. doi: 10.1371/journal.pone.0024642. URL <https://doi.org/10.1371/journal.pone.0024642>.
- Fa-Hsuan Lin, Thomas Witzel, Seppo P. Ahlfors, Steven M. Stufflebeam, John W. Belliveau, and Matti S. Hämeinen. Assessing and improving the spatial accuracy in MEG source localization by depth-weighted minimum-norm estimates. *NeuroImage*, 31(1):160–171, may 2006. ISSN 1053-8119.

- doi: 10.1016/j.neuroimage.2005.11.054. URL <http://www.sciencedirect.com/science/article/pii/S1053811905024973>.
- ChunYan Luo, XiaoYan Guo, Wei Song, Bi Zhao, Bei Cao, Jing Yang, QiYong Gong, and Hui-Fang Shang. Decreased Resting-State Interhemispheric Functional Connectivity in Parkinson's Disease. *BioMed Research International*, 2015:1–8, 2015. doi: 10.1155/2015/692684. URL <https://doi.org/10.1155/2015/692684>.
- Athen Ma and Raúl J. Mondragón. Rich-Cores in Networks. *PLOS ONE*, 10(3):e0119678, mar 2015. doi: 10.1371/journal.pone.0119678. URL <https://doi.org/10.1371/journal.pone.0119678>.
- Kanad Mandke, Jil Meier, Matthew J. Brookes, Reuben D. O'Dea, Piet Van Mieghem, Cornelis J. Stam, Arjan Hillebrand, and Prejaas Tewarie. Comparing multilayer brain networks between groups: Introducing graph metrics and recommendations. *NeuroImage*, 166:371–384, feb 2018. doi: 10.1016/j.neuroimage.2017.11.016. URL <https://doi.org/10.1016/j.neuroimage.2017.11.016>.
- Bernard Ng, Gaël Varoquaux, Jean-Baptiste Poline, and Bertrand Thirion. A Novel Sparse Graphical Approach for Multimodal Brain Connectivity Inference. In *Medical Image Computing and Computer-Assisted Intervention – MICCAI 2012*, pages 707–714. Springer Berlin Heidelberg, 2012. doi: 10.1007/978-3-642-33415-3_87. URL https://doi.org/10.1007/978-3-642-33415-3_87.
- J. B. Pochon, R. Levy, P. Fossati, S. Lehericy, J. B. Poline, B. Pillon, D. Le Bihan, and B. Dubois. The neural system that bridges reward and cognition in humans: An fMRI study. *Proceedings of the National Academy of Sciences*, 99(8):5669–5674, apr 2002. doi: 10.1073/pnas.082111099. URL <https://doi.org/10.1073/pnas.082111099>.
- Ziad T. Sankari. Local and distal coherence as a measure of cortical connectivity in Alzheimer's disease. *Alzheimer's & Dementia*, 6(4):S373, jul 2010. doi: 10.1016/j.jalz.2010.05.1250. URL <https://doi.org/10.1016/j.jalz.2010.05.1250>.
- Ernesto J. Sanz-Arigitá, Menno M. Schoonheim, Jessica S. Damoiseaux, Serge A. R. B. Rombouts, Erik Maris, Frederik Barkhof, Philip Scheltens, and Cornelis J. Stam. Loss of 'small-world' networks in Alzheimer's disease: graph analysis of FMRI resting-state functional connectivity. *PLoS One*, 5(11):e13788, November 2010. ISSN 1932-6203. doi: 10.1371/journal.pone.0013788.
- J. Schmahmann and D. Pandya. Disconnection syndromes of basal ganglia thalamus, and cerebrocerebellar systems. *Cortex*, 44(8):1037–1066, sep 2008. doi: 10.1016/j.cortex.2008.04.004. URL <https://doi.org/10.1016/j.cortex.2008.04.004>.
- Ni Shu, Xiaoni Wang, Qihui Bi, Tengda Zhao, and Ying Han. Disrupted Topologic Efficiency of White Matter Structural Connectome in Individuals with Subjective Cognitive Decline. *Radiology*, 286(1):229–238, jan 2018. doi: 10.1148/radiol.2017162696. URL <https://doi.org/10.1148/radiol.2017162696>.
- Larry R. Squire. Memory and the hippocampus: A synthesis from findings with rats monkeys, and humans: Correction. *Psychological Review*, 99(3):582–582, 1992. doi: 10.1037/0033-295x.99.3.582. URL <https://doi.org/10.1037/0033-295x.99.3.582>.
- C. J. Stam, W. de Haan, A. Daffertshofer, B. F. Jones, I. Manshanden, A. M. van Cappellen van Walsum, T. Montez, J. P. A. Verbunt, J. C. de Munck, B. W. van Dijk, H. W. Berendse, and P. Scheltens. Graph theoretical analysis of magnetoencephalographic functional connectivity in Alzheimer's disease. *Brain*, 132(1):213–224, jan 2009. ISSN 0006-8950, 1460-2156. doi: 10.1093/brain/awn262. URL <http://brain.oxfordjournals.org/content/132/1/213>.
- Cornelis J. Stam. Modern network science of neurological disorders. *Nature Reviews Neuroscience*, 15(10): 683–695, sep 2014. doi: 10.1038/nrn3801. URL <https://doi.org/10.1038/nrn3801>.
- Cornelis J. Stam, Anne Marie van Cappellen van Walsum, Yolande A. L. Pijnenburg, Henk W. Berendse, Jan C. de Munck, Philip Scheltens, and Bob W. van Dijk. Generalized synchronization of MEG recordings in Alzheimer's

- Disease: evidence for involvement of the gamma band. *J Clin Neurophysiol*, 19(6):562–574, dec 2002. ISSN 0736-0258.
- Jan-Patrick Stellmann, Sibylle Hodecker, Bastian Cheng, Nadine Wanke, Kim Lea Young, Claus Hilgetag, Christian Gerloff, Christoph Heesen, Götz Thomalla, and Susanne Siemonsen. Reduced rich-club connectivity is related to disability in primary progressive MS. *Neurology - Neuroimmunology Neuroinflammation*, 4(5):e375, jul 2017. doi: 10.1212/wnxi.0000000000000375. URL <https://doi.org/10.1212/wnxi.0000000000000375>.
- François Tadel, Sylvain Baillet, John C. Moshier, Dimitrios Pantazis, Richard M. Leahy, François Tadel, Sylvain Baillet, John C. Moshier, Dimitrios Pantazis, and Richard M. Leahy. Brainstorm: A User-Friendly Application for MEG/EEG Analysis. *Computational Intelligence and Neuroscience*, Computational Intelligence and Neuroscience, 2011, 2011:e879716, apr 2011. ISSN 1687-5265, 1687-5265. doi: 10.1155/2011/879716,10.1155/2011/879716. URL <http://www.hindawi.com/journals/cin/2011/879716/abs/>, <http://www.hindawi.com/journals/cin/2011/879716/abs/>.
- Maite Termenon, Sophie Achard, Assia Jaillard, and Chantal Delon-Martin. The “Hub Disruption Index,” a Reliable Index Sensitive to the Brain Networks Reorganization. A Study of the Contralesional Hemisphere in Stroke. *Frontiers in Computational Neuroscience*, 10, aug 2016. doi: 10.3389/fncom.2016.00084. URL <https://doi.org/10.3389/fncom.2016.00084>.
- Betty M. Tijms, Alle Meije Wink, Willem de Haan, Wiesje M. van der Flier, Cornelis J. Stam, Philip Scheltens, and Frederik Barkhof. Alzheimer's disease: connecting findings from graph theoretical studies of brain networks. *Neurobiology of Aging*, 34(8):2023–2036, aug 2013a. doi: 10.1016/j.neurobiolaging.2013.02.020. URL <https://doi.org/10.1016/j.neurobiolaging.2013.02.020>.
- Betty M. Tijms, Alle Meije Wink, Willem de Haan, Wiesje M. van der Flier, Cornelis J. Stam, Philip Scheltens, and Frederik Barkhof. Alzheimer's disease: connecting findings from graph theoretical studies of brain networks. *Neurobiol. Aging*, 34(8):2023–2036, aug 2013b. ISSN 1558-1497. doi: 10.1016/j.neurobiolaging.2013.02.020.
- Nicholas J Tustison, Brian B Avants, Philip A Cook, Yuanjie Zheng, Alexander Egan, Paul A Yushkevich, and James C Gee. N4ITK: Improved N3 Bias Correction. *IEEE Transactions on Medical Imaging*, 29(6):1310–1320, jun 2010. doi: 10.1109/tmi.2010.2046908. URL <https://doi.org/10.1109/tmi.2010.2046908>.
- Kâmil Uludağ and Alard Roebroeck. General overview on the merits of multimodal neuroimaging data fusion. *NeuroImage*, 102:3–10, nov 2014. doi: 10.1016/j.neuroimage.2014.05.018. URL <https://doi.org/10.1016/j.neuroimage.2014.05.018>.
- M. P. van den Heuvel and O. Sporns. Rich-Club Organization of the Human Connectome. *Journal of Neuroscience*, 31(44):15775–15786, nov 2011. doi: 10.1523/jneurosci.3539-11.2011. URL <https://doi.org/10.1523/jneurosci.3539-11.2011>.
- Martijn P. van den Heuvel and Olaf Sporns. Network hubs in the human brain. *Trends in Cognitive Sciences*, 17(12):683–696, dec 2013. doi: 10.1016/j.tics.2013.09.012. URL <https://doi.org/10.1016/j.tics.2013.09.012>.
- Martijn P. van den Heuvel, Olaf Sporns, Guusje Collin, Thomas Scheewe, René C. W. Mandl, Wiepke Cahn, Joaquín Goñi, Hilleke E. Hulshoff Pol, and René S. Kahn. Abnormal Rich Club Organization and Functional Brain Dynamics in Schizophrenia. *JAMA Psychiatry*, 70(8):783, aug 2013. doi: 10.1001/jamapsychiatry.2013.1328. URL <https://doi.org/10.1001/jamapsychiatry.2013.1328>.
- Tianyi Yan, Wenhui Wang, Liu Yang, Kewei Chen, Rong Chen, and Ying Han. Rich club disturbances of the human connectome from subjective cognitive decline to Alzheimer's disease. *Theranostics*, 8(12):3237–3255, 2018. doi: 10.7150/thno.23772. URL <https://doi.org/10.7150/thno.23772>.
- Tengda Zhao, Can Sheng, Qihui Bi, Weili Niu, Ni Shu, and Ying Han. Age-related differences in the topological efficiency of the brain structural connectome in amnesic mild cognitive impairment. *Neurobiology of Aging*,

59:144–155, nov 2017. doi: 10.1016/j.neurobiolaging.2017.08.005. URL <https://doi.org/10.1016%2Fj.neurobiolaging.2017.08.005>.

Tables

Table 1: Vector of the optimal layers weight for the coreness computation.

Layer m	$c^*[m]$
MEG $_{\delta}$	0.000
MEG $_{\theta}$	0.001
MEG $_{\alpha_1}$	0.258
MEG $_{\alpha_2}$	0.000
MEG $_{\beta_1}$	0.000
MEG $_{\beta_2}$	0.002
MEG $_{\gamma}$	0.000
fMRI	0.104
DWI	0.961

Figure Captions

Figure 1. **Multiplex brain network construction.** Different neuroimaging data are collected and preprocessed separately. We used the Desikan cortical atlas parcellation (Desikan et al., 2006) to infer connectivity networks from DWI, fMRI and MEG source-reconstructed data. The color of the line indicates the software that has been used in each step of the pipeline. We spatially aligned all the estimated brain networks to construct the multiplex brain network.

Figure 2. **Regional coreness of the multiplex brain networks.** Panel **a)**, shows the results of the particle swarm optimization (PSO) used to find the best layer coefficients vector c that maximizes the Fisher score $F(c)$ between AD and HC subjects. In the upper plot, each dot represents the position of a particle at a given iteration in the original 9-dimension coreness contribution coefficient vector space. The color of the dots code for the corresponding Fisher score. Results were projected over the three main network layers for the sake of illustration. The other non-shown components were rapidly zeroing-out during the 81 iterations needed to converge to the optimum as shown in the bottom plot. Panel **b)** shows the corresponding average coreness for the healthy control (HC) population and for the Alzheimer's disease (AD) group. The position of the nodes identifies the barycentre of each ROI in the cortical surface here represented in transparent grey; the color of each node codes for the average coreness \bar{C}_i .

Figure 3. **Differences in regional coreness between AD and HC subjects.** Panel **a)** shows the between-group difference of coreness $\bar{C}_{AD,i} - \bar{C}_{HC,i}$ as a function of the healthy population's coreness $\bar{C}_{HC,i}$; the slope of the regression line in grey measures the coreness disruption index $\kappa = -0.20$. The color of the circles code for the difference between average coreness in the AD and HC group; stars point out the ROIs for which we reported a significant difference ($p < 0.025$), Supplementary Table 2). Panel **b)** illustrates the values of the between-group coreness difference over the Desikan cortical atlas. Color code is the same in Panel **a)**.

Figure 4. **Coreness disruption index as a function of network randomization.** Boxplots show the values of coreness disruption index (κ) obtained by randomly rewiring an increasing percentage of links in the multiplex brain networks of the HC group (see Materials and methods for more details). For example, RA₁₅ means that 15% of the links were reshuffled randomly in each layer. The blue and red boxplots illustrate respectively the κ values for the HC and AD group. The circles in the boxes show the median; the bottom and top edges of the boxes denote the 25th and 75th percentile, respectively. Whiskers connect the most extreme points not considered outliers, and outliers are plotted individually as circles.

Figure 5. **Correlation between coreness and cognitive/memory deficit.** Panel **a)** show the values of the minimal state examination (MMSE) and immediate recall (IR) as a function of the coreness disruption index κ . In panel **b)** the Spearman correlation values (R) between the regional coreness C_i and the MMSE and IR values are shown over the Desikan cortical atlas.

Figures

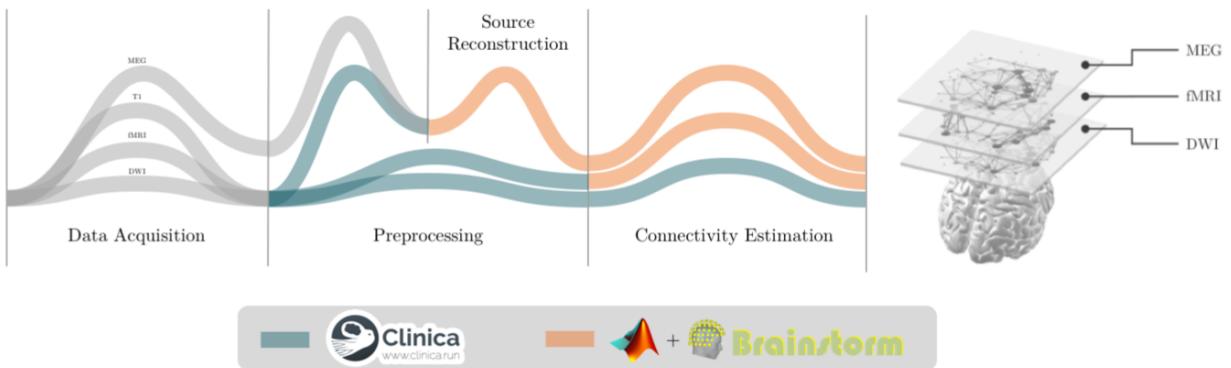


Figure 1: **Multiplex brain network construction.** Different neuroimaging data are collected and preprocessed separately. We used the Desikan cortical atlas parcellation (Desikan et al., 2006) to infer connectivity networks from DWI, fMRI and MEG source-reconstructed data. The color of the line indicates the software that has been used in each step of the pipeline. We spatially aligned all the estimated brain networks to construct the multiplex brain network.

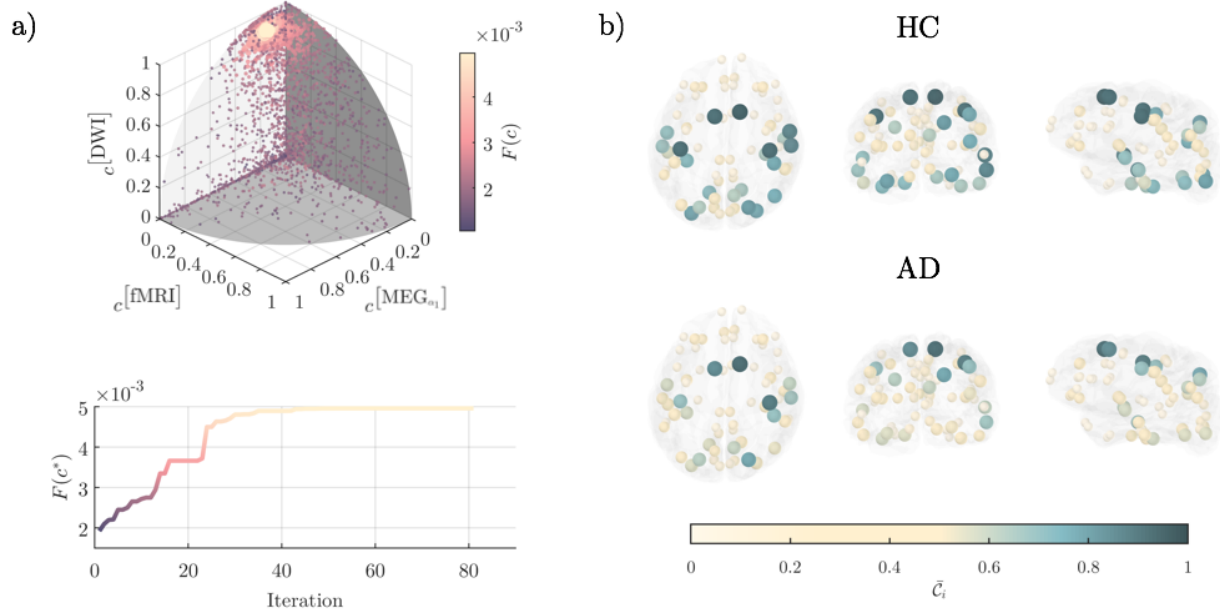


Figure 2: **Regional coreness of the multiplex brain networks.** Panel **a)**, shows the results of the particle swarm optimization (PSO) used to find the best layer coefficients vector c that maximizes the Fisher score $F(c)$ between AD and HC subjects. In the upper plot, each dot represents the position of a particle at a given iteration in the original 9-dimension coreness contribution coefficient vector space. The color of the dots code for the corresponding Fisher score. Results were projected over the three main network layers for the sake of illustration. The other non-shown components were rapidly zeroing-out during the 81 iterations needed to converge to the optimum as shown in the bottom plot. Panel **b)** shows the corresponding average coreness for the healthy control (HC) population and for the Alzheimer's disease (AD) group. The position of the nodes identifies the barycentre of each ROI in the cortical surface here represented in transparent grey; the color of each node codes for the average coreness \bar{C}_i .

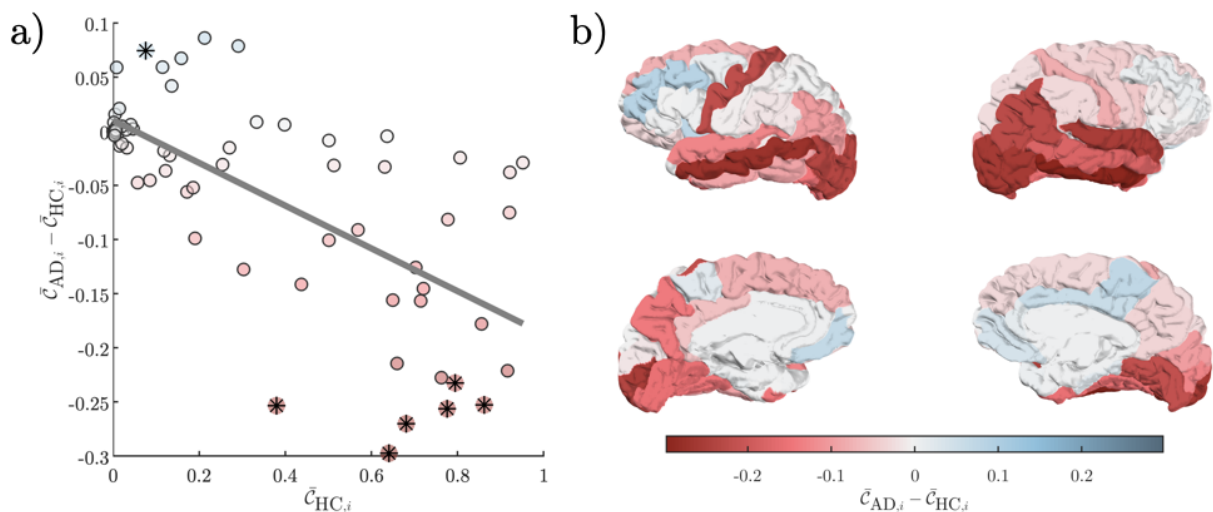


Figure 3: **Differences in regional coreness between AD and HC subjects.** Panel a) shows the between-group difference of coreness $\bar{C}_{AD,i} - \bar{C}_{HC,i}$ as a function of the healthy population's coreness $\bar{C}_{HC,i}$; the slope of the regression line in grey measures the coreness disruption index $\kappa = -0.20$. The color of the circles code for the difference between average coreness in the AD and HC group; stars point out the ROIs for which we reported a significant difference ($p < 0.025$), Supplementary Table 2). Panel b) illustrates the values of the between-group coreness difference over the Desikan cortical atlas. Color code is the same in Panel a).

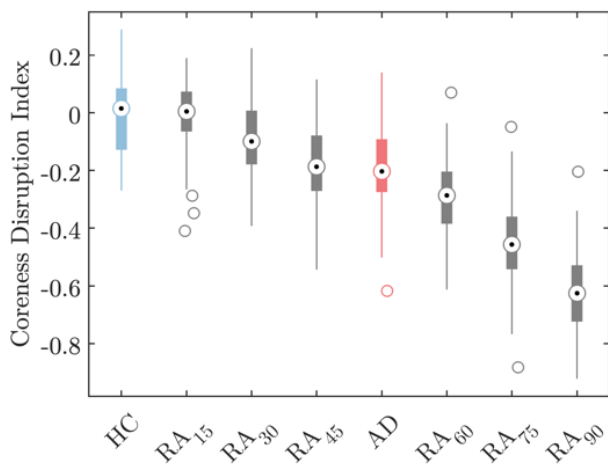


Figure 4: **Coreness disruption index as a function of network randomization.** Boxplots show the values of coreness disruption index (κ) obtained by randomly rewiring an increasing percentage of links in the multiplex brain networks of the HC group (see Materials and methods for more details). For example, RA₁₅ means that 15% of the links were reshuffled randomly in each layer. The blue and red boxplots illustrate respectively the κ values for the HC and AD group. The circles in the boxes show the median; the bottom and top edges of the boxes denote the 25th and 75th percentile, respectively. Whiskers connect the most extreme points not considered outliers, and outliers are plotted individually as circles.

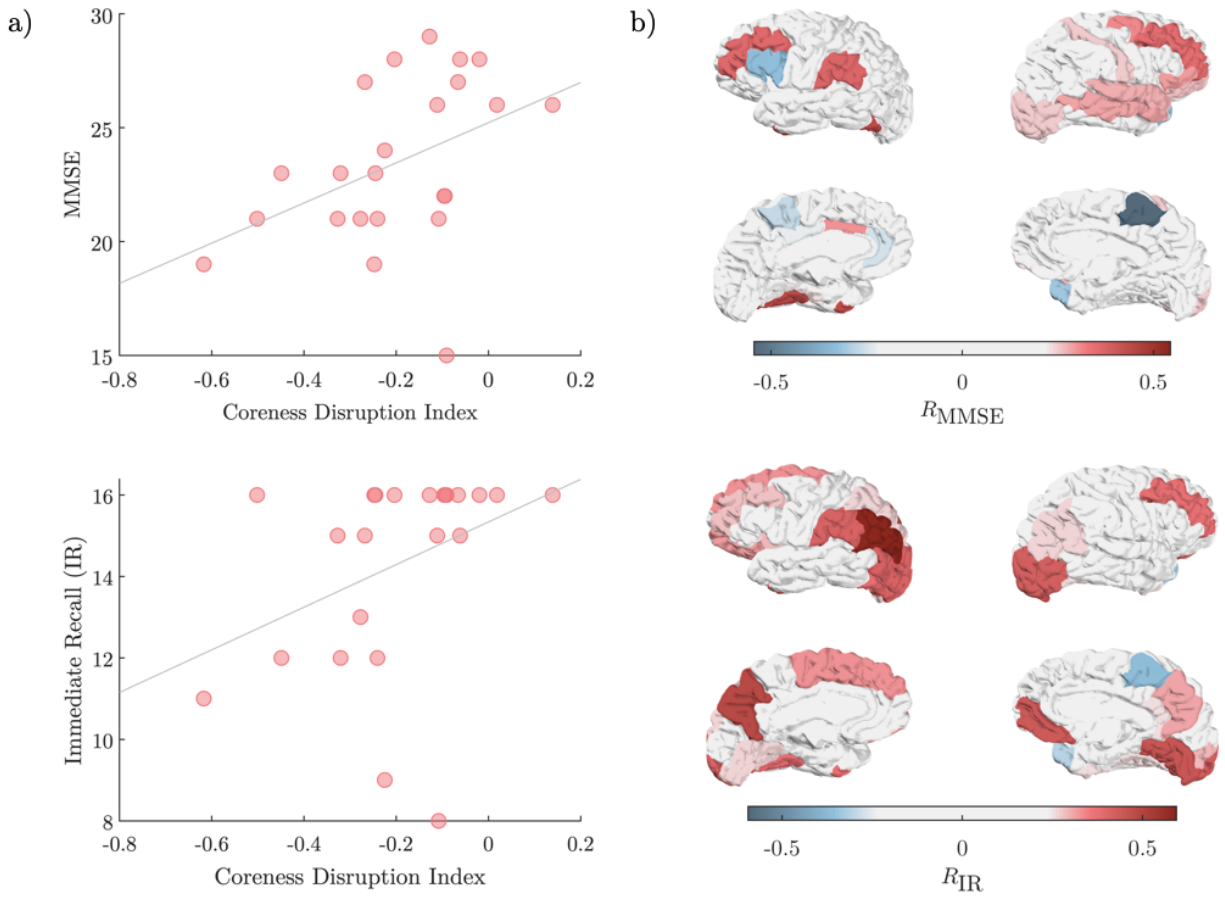


Figure 5: **Correlation between coreness and cognitive/memory deficit.** Panel a) show the values of the mini-mental state examination (MMSE) and immediate recall (IR) as a function of the coreness disruption index κ . In panel b) the Spearman correlation values (R) between the regional coreness \mathcal{C}_i and the MMSE and IR values are shown over the Desikan cortical atlas.

Disrupted core-periphery structure of multimodal brain networks in Alzheimer's Disease (Supplementary Material)

Jeremy Guillon^{1,2}, Mario Chavez³, Federico Battiston^{10,3,2}, Yohan Attal⁴, Valentina La Corte^{5,6,7}, Michel Thiebaut de Schotten¹, Bruno Dubois⁸, Denis Schwartz⁹, Olivier Colliot^{2,1}, and Fabrizio De Vico Fallani^{2,1,*}

¹Institut du Cerveau et de la Moelle Epiniere, ICM, Inserm, U 1127, CNRS, UMR 7225, Sorbonne Universite, F-75013, Paris, France

²Inria Paris, Aramis project-team, F-75013, Paris, France

³CNRS, UMR 7225, F-75013, Paris, France

⁴MyBrain Technologies, Paris, France

⁵Department of Neurology, Institut de la Memoire et de la Maladie d'Alzheimer - IM2A, Paris, France

⁶INSERM UMR 894, Center of Psychiatry and Neurosciences, Memory and Cognition Laboratory, Paris, France

⁷Institute of Psychology, University Paris Descartes, Sorbonne Paris Cite, France

⁸Institut de la Mémoire et de la Maladie d'Alzheimer - IM2A, AP-HP, Sorbonne Université, Paris, France

⁹Institut du Cerveau et de la Moelle Epiniere, ICM, Inserm U 1127, CNRS UMR 7225, Sorbonne Universite, Ecole Normale Supérieure, ENS, Centre MEG-EEG, F-75013, Paris, France

¹⁰Department of Network and Data Science, Central European University, Budapest 1051, Hungary

*Corresponding author

December 10, 2018

Supplementary material

Supplementary figure

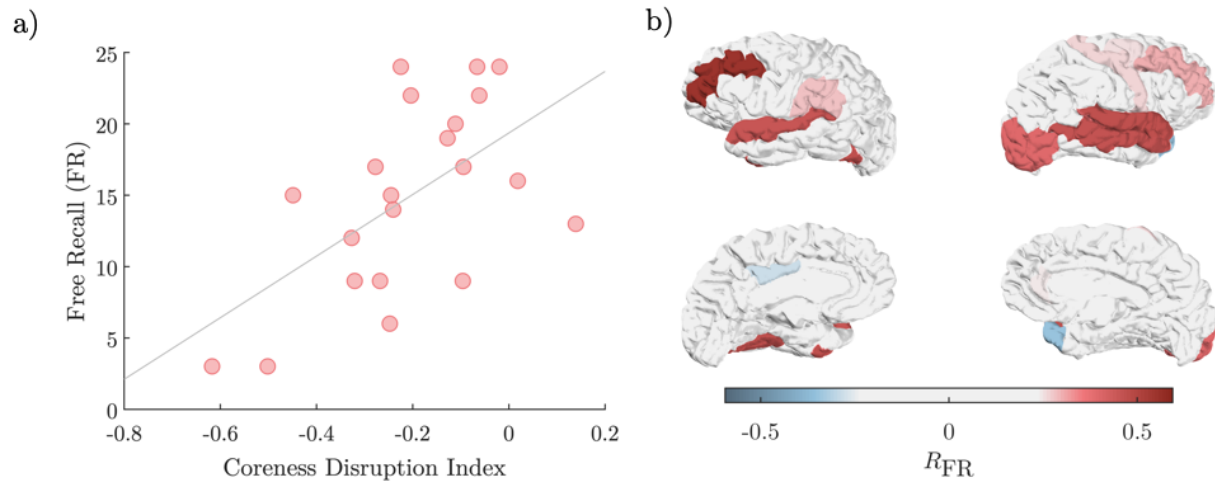


Figure S1: **Correlation between coreness and cognitive/memory deficit.** Panel **a)** shows the values of the free recall (FR) as a function of the coreness disruption index κ . In panel **b)** the Spearman correlation values (R_{FR}) between the regional coreness C_i and the FR values are shown over the Desikan cortical atlas.

Supplementary tables

Table S1: ADs population coreness disruption indices κ and the associated R^2 of the linear regression.

Subject ID	κ	R^2
1	-0,095	0,018
2	-0,111	0,033
3	-0,096	0,019
4	0,139	0,040
5	-0,502	0,412
6	0,018	0,001
7	-0,327	0,218
8	-0,617	0,267
9	-0,241	0,106
10	-0,062	0,015
11	-0,204	0,099
12	-0,245	0,085
13	-0,225	0,056
14	-0,020	0,001
15	-0,128	0,019
16	-0,248	0,141
17	-0,268	0,106
18	-0,278	0,081
19	-0,449	0,387
20	-0,091	0,011
21	-0,108	0,025
22	-0,320	0,258
23	-0,066	0,014

Table S2: Average coreness differences and their associated p -value. Ordered in descending $\bar{C}_{HC,i}$. Significant values ($\alpha_{FDR} = 0,025$) are in bold.

Label	$\bar{C}_{AD,i}$	$\bar{C}_{HC,i}$	$\bar{C}_{AD,i} - \bar{C}_{HC,i}$	p -Value
superiorfrontal R	0,923	0,952	-0,029	0,743
precentral R	0,883	0,921	-0,038	0,719
superiorfrontal L	0,846	0,921	-0,075	0,579
precentral L	0,695	0,916	-0,221	0,543
superiortemporal R	0,609	0,862	-0,253	0,005
middletemporal R	0,677	0,855	-0,178	0,121
superioparietal R	0,781	0,806	-0,025	0,650
lateraloccipital L	0,562	0,794	-0,233	0,020
postcentral R	0,696	0,778	-0,082	0,613
lateraloccipital R	0,520	0,776	-0,256	0,008
inferioparietal R	0,535	0,763	-0,228	0,071
fusiform L	0,575	0,720	-0,145	0,133
lingual L	0,558	0,715	-0,157	0,210
superiortemporal L	0,577	0,703	-0,126	0,316
middletemporal L	0,411	0,681	-0,270	0,017
lingual R	0,445	0,660	-0,214	0,034
fusiform R	0,494	0,650	-0,156	0,203
inferiortemporal R	0,344	0,641	-0,297	0,002
superioparietal L	0,632	0,637	-0,005	0,992
precuneus R	0,598	0,631	-0,033	0,756
inferiortemporal L	0,478	0,569	-0,091	0,288
supramarginal R	0,482	0,513	-0,032	0,674
inferioparietal L	0,401	0,502	-0,101	0,279
postcentral L	0,493	0,501	-0,009	0,787
precuneus L	0,296	0,437	-0,142	0,173
insula R	0,404	0,398	0,006	0,666
pericalcarine L	0,126	0,379	-0,254	0,012
rostralmiddlefrontal R	0,342	0,334	0,008	0,880
pericalcarine R	0,176	0,304	-0,128	0,151
insula L	0,369	0,290	0,079	0,388
supramarginal L	0,255	0,270	-0,015	0,771
lateralorbitofrontal L	0,223	0,254	-0,031	0,747
rostralmiddlefrontal L	0,299	0,213	0,086	0,349
cuneus R	0,091	0,191	-0,099	0,391
isthmuscingulate L	0,134	0,186	-0,052	0,324
posteriorcingulate L	0,116	0,172	-0,056	0,559
medialorbitofrontal L	0,226	0,158	0,067	0,221
medialorbitofrontal R	0,178	0,136	0,042	0,709
lateralorbitofrontal R	0,109	0,131	-0,022	0,696
isthmuscingulate R	0,086	0,122	-0,037	0,907
cuneus L	0,100	0,118	-0,018	0,201
posteriorcingulate R	0,174	0,115	0,059	0,192
caudalmiddlefrontal R	0,040	0,086	-0,045	0,966
paracentral R	0,151	0,076	0,074	0,022
parsopectoralis R	0,010	0,057	-0,048	0,337
parsopectoralis L	0,049	0,046	0,002	1,000
caudalmiddlefrontal L	0,047	0,041	0,006	0,946
bankssts R	0,018	0,033	-0,015	0,326
rostralanteriorcingulate L	0,032	0,031	0,001	0,568
bankssts L	0,010	0,021	-0,012	0,588
parahippocampal L	0,025	0,021	0,005	0,928
parstriangularis R	0,002	0,015	-0,014	0,754
paracentral L	0,036	0,015	0,021	0,462
parahippocampal R	0,035	0,014	0,021	0,679
parstriangularis L	0,007	0,010	-0,003	0,909
caudalanteriorcingulate L	0,014	0,009	0,004	0,629
caudalanteriorcingulate R	0,067	0,008	0,059	0,929
temporalpole L	0,008	0,007	0,001	0,805
rostralanteriorcingulate R	0,021	0,005	0,016	0,264
entorhinal L	0,004	0,005	-0,001	0,399
transversetemporal L	0,000	0,004	-0,004	0,189
frontalpole L	0,000	0,003	-0,003	0,368
parsorbitalis L	0,004	0,003	0,001	0,874
temporalpole R	0,010	0,002	0,008	0,682
parsorbitalis R	0,001	0,002	-0,002	0,630
transversetemporal R	0,001	0,002	-0,002	0,630
entorhinal R	0,000	0,000	0,000	NA
frontalpole R	0,000	0,000	0,000	NA